Evaluation of the applicability of the dual-domain mass transfer model in porous media containing connected high-conductivity channels

Gaisheng Liu,[1] Chunmiao Zheng,[2] and Steven M. Gorelick[3]

Received 10 February 2007; revised 15 August 2007; accepted 19 September 2007; published 20 December 2007.

[1] This paper evaluates the dual-domain mass transfer (DDMT) model to represent transport processes when small-scale high-conductivity (K) preferential flow paths (PFPs) are present in a homogenous porous media matrix. The effects of PFPs upon solute transport were examined through detailed numerical experiments involving different realizations of PFP networks, PFP/matrix conductivity contrasts varying from 10:1 to 200:1, different magnitudes of effective conductivities, and a range of molecular diffusion coefficients. Results suggest that the DDMT model can reproduce both the near-source peak and the downstream low-concentration spreading observed in the embedded dendritic network when there are large conductivity contrasts between high-K PFPs and the low-K matrix. The accuracy of the DDMT model is also affected by the geometry of PFP networks and by the relative significance of the diffusion process in the network-matrix system.

Citation: Liu, G., C. Zheng, and S. M. Gorelick (2007), Evaluation of the applicability of the dual-domain mass transfer model in porous media containing connected high-conductivity channels, *Water Resour. Res.*, *43*, W12407, doi:10.1029/2007WR005965.

1. Introduction

[2] Small-scale preferential flow paths (PFPs) are believed to exert a strong influence on solute transport on field-scale transport at the MADE site located on the Columbus Air Force Base in Mississippi [*Boggs and Adams*, 1992; *Boggs et al.*, 1993; *Zheng and Jiao*, 1998; *Feehley et al.*, 2000; *Harvey and Gorelick*, 2000]. Due to the extreme aquifer heterogeneity and likely occurrence of small-scale PFPs at the site, the observed concentration profiles of nonreactive tracers, i.e., bromide in the first experiment (MADE-1) and tritium in the second experiment (MADE-2), exhibit highly non-Gaussian patterns with a near-source peak and extensive spreading to the far-field in low concentrations [*Boggs et al.*, 1992, 1993]. The observed plume distribution could not be represented using the standard advective-dispersive equation [*Feehley et al.*, 2000; *Harvey and Gorelick*, 2000], although this matter has been recently debated [*Barlebo et al.*, 2004; *Molz et al.*, 2006; *Hill et al.*, 2006].

[3] The dual-domain mass transfer (DDMT) approach is able to reproduce the near-source peak as well as the extensive solute spreading downgradient at low concentrations. Using a DDMT model, *Harvey and Gorelick* [2000] explained the change in observed plume mass with time at the MADE site, a phenomenon that had been previously attributed to experimental errors. *Haggerty et al.* [2001] applied a DDMT model to investigate the observed behavior in a series of single-well injection-withdrawal tests conducted in a fractured dolomite. Considering that the mass exchange in natural heterogeneous media may be a consequence of different mass transfer rates, the DDMT approach was also extended to consider multidomain [*Gwo et al.*, 1995], multiphase [*Falta*, 2000] and multirate [*Haggerty and Gorelick*, 1995; *McKenna et al.*, 2001; *Wang et al.*, 2005] transport.

[4] In aquifers containing high-K PFPs, transport can be divided into two domains: a relatively mobile domain (i.e., the PFPs) where advection is enhanced, and a relatively immobile region where the rate of advection can be several orders of magnitude smaller compared to that in the relatively mobile domain. The rate-limited mass transfer process between the two domains is controlled by molecular diffusion and slow advection across the mobile-immobile domain interface. The latter factor is further dependent on the geometry of PFPs and the magnitude of the conductivity contrast between the PFPs and the relative immobile flow barriers. Theoretically, if the spatial distribution of these small-scale PFPs were fully defined and a numerical model grid were sufficiently refined to permit explicit representation of the PFPs, transport could be characterized accurately by an advection-diffusion model. In practice, however, this is generally precluded both by a lack of detailed field data and by extreme computational requirements [*Zheng and Bennett*, 2002]. Thus the effects of small-scale PFPs on solute transport are often accounted for using models that treat the system in an upscaled manner. In this study, we evaluate the applicability of the DDMT model to represent the small-scale PFPs under various conditions.

[5] It is noteworthy that other novel theories have also been developed to describe transport controlled by small-

[1]Kansas Geological Survey, University of Kansas, Lawrence, Kansas, USA.
[2]Department of Geological Sciences, University of Alabama, Tuscaloosa, Alabama, USA.
[3]Department of Environmental Earth System Science, Stanford University, Stanford, California, USA.

0043-1397/07/2007WR005965

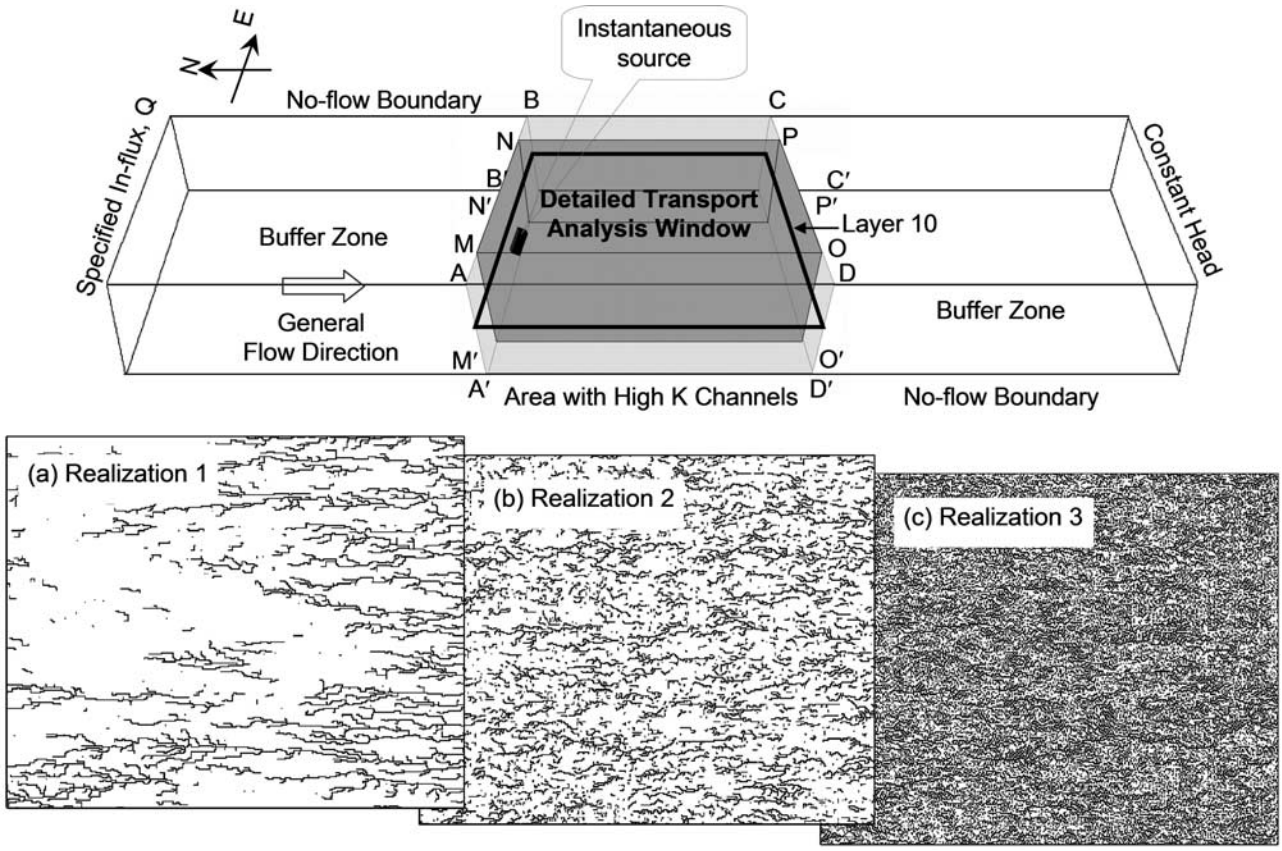

Figure 1. Schematic diagram of 3-D synthetic-aquifer model. Also shown are the PFP images at layer 10 of the detailed transport analysis window: (a) PFP network realization 1, (b) PFP network realization 2, and (c) PFP network realization 3. The volumetric fraction of PFPs is ~9% in realization 1, ~20% in realization 2, and ~46% in realization 3.

scale heterogeneities [*Berkowitz and Scher*, 1998; *Benson et al.*, 2000]. *Berkowitz et al.* [2002, 2006] provide some theoretical insights among various transport formalisms and demonstrate that these different approaches may be unified under the general framework of continuous time random walk. Anomalous transport behavior has also been observed in catchments [*Kirchner et al.*, 2000; *Scher et al.*, 2002].

[6] Here we report the results of numerical experiments conducted on a 3-D synthetic aquifer containing decimeter-scale high-K "channels" (i.e., PFPs) embedded in a low-conductivity "matrix." The hypothetical 3-D PFP networks are generated using an invasion percolation algorithm [*Liu et al.*, 2004]. The effective hydraulic properties of such networks in 2-D were investigated by *Ronayne and Gorelick* [2006]. Given the explicit representation of these decimeter-scale PFPs, solute transport is systematically examined under a variety of flow and transport conditions. The key question we seek to answer is whether or not the DDMT model can be applied to satisfactorily simulate solute transport processes in aquifers containing fine-scale PFPs under varied conditions. Major factors that dictate the applicability of the DDMT model are explored, including the conductivity contrast between the PFPs and the matrix, molecular diffusion, and different geometries of PFPs.

[7] The PFPs examined in this study are intended to provide one possible representation of permeable interconnected structures even if many others are possible. The dendritic patterns that we represent may be applicable to karst systems as well as other porous media environments. We merely use this particular system as a convenient construct to explore the case of tortuous connected pathways that are embedded in a permeable matrix. We note that the PFPs in fractured bedrock are quite different in that our matrix is much more permeable than bedrock even under the highest K contrast we consider.

2. Methodology

[8] To determine the viability of the DDMT model in representing transport processes in aquifers containing small-scale PFPs, we conducted a series of numerical experiments using the flow and transport codes MOFLOW-2000 [*Harbaugh et al.*, 2000] and MT3DMS [*Zheng and Wang*, 1999; *Zheng*, 2006]. First, advection-diffusion processes were simulated in great detail in a binary 3-D PFP-matrix flow system (Figure 1). The solute plumes were obtained for different PFP/matrix conductivity contrasts, effective conductivity values, molecular diffusion coefficients, and PFP network geometries. These are the same model systems that were used to explore the applicability of the classical advective-dispersive equation from *Liu et al.* [2004]. The generated plumes are then used as the "true" references for comparison with those resulting from the equivalent DDMT model applied to each case. The DDMT model consists of an advective-dispersive transport equation for solutes in the mobile fluid zone coupled with a mass transfer equation that

describes the mass exchange between the mobile and immobile fluid zones.

2.1. PFP Network Advection-Diffusion Model

[9] The advection-diffusion equation describing the fate and transport of conservative solutes in 3-D groundwater flow systems can be expressed in subscript form as

$$\frac{\partial(nC)}{\partial t} = \frac{\partial}{\partial x_i}\left(nD * \frac{\partial C}{\partial x_i}\right) - \frac{\partial}{\partial x_i}(q_i C) + q_s C_s, \qquad (1)$$

where C is the dissolved solute concentration; n is the porosity of the porous media; D^* is the molecular diffusion coefficient in porous media; q_i is the ith component of the specific discharge; and C_s is the concentration of the fluid source/sink flux q_s.

[10] The basic flow and transport model setup is sketched in Figure 1. The flow domain is 200 m long by 51.2 m wide by 2 m thick and discretized into 20 layers. Each layer is 10 cm thick and consists of 512 columns and 430 rows. The area ABCD-ABCD is the region where the high-K PFPs are embedded within the low-K matrix. The high-K PFPs are assumed 10 cm wide. Preliminary simulations indicated that the representation of 10 cm-wide channels with 10 cm-wide cells is sufficiently accurate for the purposes of this study. The PFP network used in this study was generated using an invasion percolation algorithm based on *Stark* [1991]. Further details regarding the numerical model, the percolation algorithm, and the realizations generated are given by *Liu et al.* [2004] and *Gorelick et al.* [2005]; we employ the same system and realizations in this study.

[11] The aquifer is confined and the flow field is steady state. There is no groundwater flow across the eastern and western boundaries. The southern boundary is constant-head. The northern boundary is a specified-flux with the groundwater inflow (Q) so determined as to achieve an average hydraulic gradient of 0.001 in the dominant flow direction. To minimize the boundary effects, the area ABCD-A′B′C′D′ is set sufficiently far away from the northern and southern borders throughflow buffer zones. The grid spacing in PFP-matrix area ABCD-A′B′C′D′ is 10 cm in both row (east-west) and column (north-south) directions. Detailed solute transport analysis is conducted in a smaller window (MNOP-M′N′O′P′ in Figure 1) inside the area ABCD-A′B′C′D′. Transport boundary conditions are zero concentration gradient across all sides of the transport analysis window. The source placement configuration examined here is a zone of 7 m wide, 0.4 m deep and 0.4 m extended in the direction of flow, within which initial mass is non-uniformly distributed in proportion to the respective K values. This "partitioned" source represents the distribution of solutes in the aquifer where the PFPs receive a higher amount of injected mass than the matrix in proportion to the ratio of PFP/matrix K values during an instantaneous tracer injection event. The source area occupies 4.7% of the total area perpendicular to mean flow.

[12] Only advection and molecular diffusion are modeled when considering the full 3-D embedded PFP network. The diffusion coefficient is 8.64×10^{-6} m^2/day unless stated otherwise. Local pore-scale dispersion is not included. To achieve this full representation of the decimeter-scale high-K PFPs, 4.4 million cells are used in the flow and transport simulations. Practically, the effects of small-scale high-K PFPs must be represented in an upscaled manner in field situations.

2.2. Dual-Domain Mass Transfer (DDMT) Model

[13] In this study we consider the efficacy of the DDMT model for representing transport processes in the PFP networks. The DDMT system is conceptualized as consisting of two domains: a mobile zone with pore spaces filled with mobile water where transport is primarily by advection; and an immobile zone with pore spaces filled with stagnant water where advective transport is negligible. Solute exchange between the mobile and immobile fluid zones is driven by the concentration difference between the two domains. The governing equations for the DDMT model can be expressed for conservative solutes as [*Feehley et al.*, 2000; *Gorelick et al.*, 2005]

$$n_m \frac{\partial C_m}{\partial t} + n_{im} \frac{\partial C_{im}}{\partial t} = \frac{\partial}{\partial x_i}\left(n_m D_{ij} \frac{\partial C_m}{\partial x_j}\right) - \frac{\partial}{\partial x_i}(q_i C_m) + q_s C_s, \qquad (2a)$$

$$n_{im} \frac{\partial C_{im}}{\partial t} = \xi(C_m - C_{im}), \qquad (2b)$$

where C_m and n_m are the concentration and porosity in the mobile domain; C_{im} and n_{im} are the concentration and porosity in the immobile domain; and ξ is the first-order mass transfer rate. Note that with equation (2b), the mass transfer between the mobile and immobile zones is approximated by a linear non-equilibrium model. D_{ij} is the dispersion coefficient. To account for more complex field conditions, a higher-order diffusion or first-order multirate equation may be applied [*Haggerty and Gorelick*, 1995].

[14] In the DDMT model, solute is transported by advection through the high-K mobile zone, while no advection occurs in the low-K matrix immobile zone. The immobile zone essentially acts as a sink or source for solutes in the mobile zone depending on the direction of the concentration gradient between the two zones. It is noteworthy that in the DDMT model, it is assumed that no advective transport occurs in the immobile zone; but in the true PFP network model advection may still be present in the matrix though at a slower rate. Thus there is always a discrepancy using the DDMT approach because relatively low-velocity flow zones are approximated as absolutely immobile zones. In the DDMT model we consider local-scale, sub-grid dispersion as an additional process that can occur. Numerical experiments showed that results were not affected by local scale longitudinal dispersivity, so it was set equal to zero. The nominal values of local-scale dispersivities in the transverse directions were determined by spatial moment analysis [*Liu et al.*, 2004, equation (11)].

[15] The DDMT model has two additional parameters, the mobile versus total porosity ratio Φ, where $\Phi = n_m/(n_m + n_{im})$, and the mass transfer rate coefficient ξ between mobile and immobile zones. In general, these parameters are determined indirectly by matching simulated concentrations to observed tracer data [*Feehley et al.*, 2000; *Harvey and Gorelick*, 2000; *Haggerty et al.*, 2001]. For the synthetic PFP network-matrix systems considered in this work, how-

ever, in the following sections we show that they can be directly estimated using physically derived formulae without resorting to model calibration.

[16] Here we present the logic leading to the development of the relationship between the mobile porosity ratio and the hydraulic conductivities of the PFP network-matrix system. To determine the mobile porosity ratio, consider that the DDMT system can be conceptually treated as straight mobile and immobile strips aligned along the ambient flow direction. Accordingly, we conceptualize the dendritic PFP network system as straight PFP conduits embedded in the homogeneous low-K matrix. Imagine that the straight conduits have the same properties as the dendritic PFPs (i.e., conductivity and porosity). To obtain the equivalency between the dendritic network and straight PFP conduits, the total flow rate must remain identical under the same hydraulic gradient. Applying Darcy's law to both the dendritic and straight conduit systems, respectively, one obtains

$$K_N IA = RK_C IA + (1-R)K_M IA, \tag{3}$$

where I is the mean hydraulic gradient; A is the cross-sectional area of the entire system; K_M is the matrix conductivity; K_C is the conductivity of PFPs; K_N is the effective conductivity (the average hydraulic conductivity value that preserves total discharge) of the dendritic PFP network-matrix system, which is easily determined using the flow model once K_M and K_C are known; and R is the volumetric fraction of straight PFP conduits. The first, second and third terms of (3) are the total flow rates for the dendritic system, the straight PFP conduits, and the low-K matrix between the straight conduits, respectively. It is noteworthy that in the dendritic network system, the flow in the PFPs and low-K matrix is integrated through the single effective conductivity term, K_N.

[17] As a conceptual approximation of the dendritic network system in this development, we treat the straight PFP conduits as the mobile strips and the low-K matrix as the immobile strips in the DDMT model. Because the PFPs and low-K matrix are assumed to have the same porosity of 0.2 here, the fraction of mobile porosity Φ in the DDMT model is equivalent to the volumetric percentage of straight PFP conduits relative to the total porosity ($n_m + n_{im}$) set equal to 0.2. From (3), the mobile porosity fraction is calculated as

$$\Phi = R = \frac{K_N - K_M}{K_C - K_M}. \tag{4}$$

Note that during the above derivation, we approximate the low-K matrix with conductivity K_M as the absolutely immobile strips with zero conductivity in the DDMT model. As demonstrated in the following sections, the error associated with this approximation may or may not be significant, depending mainly on the PFP/matrix conductivity contrast.

[18] The mass transfer rate coefficient used in the DDMT model is calculated as [*Gorelick et al.*, 2005]

$$\xi = (\beta)\left[\left(\frac{(D/L)}{\Delta V_{KNR}} + \frac{K_M}{K_N - K_R}\right) \times \left(\frac{f_c - \Phi}{\Phi}\right)\right], \tag{5}$$

where $\Delta V_{KNR} = |V_{KN} - V_{KR}|$, which is the difference between average velocity, V_{KN}, in the entire embedded dendritic network system and the average velocity, V_{KR}, in a completely random (binary) heterogeneous conductivity field consisting of the same materials as the dendritic PFP network (i.e., the PFP volume is randomly distributed within the low-conductivity matrix rather than being connected); K_R is the effective conductivity of the random field. D is the product of mobile porosity and molecular diffusion coefficient, $n_m D^*$; L is the representative width of PFPs, here taken to be 10 cm; f_c is the volume fraction of high-K PFPs. Of importance, ΔV_{KNR} describes the degree to which flow occurs in preferential pathways in structures containing a PFP network versus flow that occurs through comparable randomized structures with few connected pathways. It essentially provides a measure of the relative connectivity of PFPs, The value of the constant β, which has the same units as ξ, was determined previously by fitting to be 0.001875 d^{-1} [*Gorelick et al.*, 2005].

[19] Equation (5) not only yields ξ, but also provides insight into the nature of the mass transfer processes [*Gorelick et al.*, 2005]. The first and second terms in the square bracket (i.e., $\frac{(D/L)}{\Delta V_{KNR}}$ and $\frac{K_M}{K_N - K_R}$) consider the relative significance of diffusion and matrix-limiting advection, respectively. The first term is essentially an inverse Peclet number. The second term is akin to a Courant number for the case of steady flow under a specified hydraulic gradient, which cancels in the numerator and denominator written in terms of the groundwater velocity equation. This term describes the velocity in the matrix relative to velocity through the PFP minus that in a completely random binary conductivity field. The third term (i.e., $\frac{f_c - \Phi}{\Phi}$) is a normalization factor to accommodate different PFP volumetric percentages in the network system and different mobile zone fractions used in the DDMT model. From (5), smaller values of effective mass transfer coefficients correspond typically to larger conduit-matrix conductivity contrasts, smaller values of diffusion coefficients, greater network connectivity, and lower conduit-volume fractions.

2.3. Model Evaluation Criterion

[20] Quantitative comparison between the two model predictions is made by computing the root-mean-square error (*RMSE*) between the plumes simulated through the true PFP network system and the plumes simulated by the equivalent DDMT model,

$$RMSE = \sqrt{\frac{1}{NROW}\sum_{i=1}^{NROW}\left[\log\left[M_{1,i}/M_0\right] - \log\left[M_{2,i}/M_0\right]\right]^2}, \tag{6}$$

where M_0 is the initial source mass; $M_{1,i}$ and $M_{2,i}$ are the solute mass in the PFP-network system and that simulated by the DDMT model at location i, respectively,

$$M_{p,i}/M_0 = \sum_{k=1}^{NLAY}\sum_{j=1}^{NCOL} C_p(j,i,k) \times V(j,i,k)/M_0, \tag{7}$$

where p is either 1 to indicate the PFP-network system or 2 to indicate the DDMT model; *NROW*, *NCOL* and *NLAY* are the total numbers of row, columns and layers, which are 370, 300 and 20, respectively, of the detailed solute

Table 1. Summary Statistics of Conductivity Field at Different Conductivity Contrasts for PFP Network Realization 1[a]

K Ratio	Model K Values	Mean K	Var K	Mean (lnK)	Var (lnK)
10:1	PFP, 8.34 Matrix, 0.84	1.51	4.63	0.03	0.44
15:1	PFP, 10.76 Matrix, 0.72	1.62	8.29	−0.09	0.60
20:1	PFP, 12.66 Matrix, 0.63	1.72	11.87	−0.19	0.74
30:1	PFP, 15.48 Matrix, 0.52	1.87	18.40	−0.35	0.95
50:1	PFP,19.14 Matrix,0.38	2.08	28.90	−0.61	1.26
100:1	PFP, 24 Matrix, 0.24	2.38	46.36	−1.01	1.74
150:1	PFP, 26.75 Matrix, 0.18	2.58	57.97	−1.27	2.06
200:1	PFP, 28.68 Matrix, 0.14	2.72	66.87	−1.46	2.31

[a]K values are in m/d.

transport analysis window (MNOP-M′N′O′P′ in Figure 1); and $V(j, i, k)$ and $C(j, i, k)$ are the pore water volume and concentration at cell (j, i, k). Note that the row direction (index i) is perpendicular to the mean flow. Because the DDMT model is intended to represent the bulk behavior of PFP network transport, it is more meaningful to use the integrated mass profiles as expressed in (7) in computing the *RMSE* so that the local effects of cell-to-cell mismatch would not skew the comparison. By taking the log transformation in (6), the *RMSE* provides an unbiased statistical indicator in that the transport characteristics in both the high-concentration plume center and low-concentration plume edges are appropriately accounted for. For $M_{p,i}/M_0$ below a minimum threshold value of 10^{-6}, the mass at the ith row is considered indistinguishable from zero and $\log[M_{p,i}/M_0]$ is set equal to -6.

[21] Note that for the DDMT model, as each cell consists of mobile and immobile domains, $C_2(j, i, k)$ is computed as

$$C_2(j,i,k) = \Phi C_m(j,i,k) + (1-\Phi)C_m(j,i,k), \tag{8}$$

where $C_m(j, i, k)$ and $C_{im}(j, i, k)$ are the concentrations in the mobile and immobile domains at cell (j, i, k).

[22] The *RMSE* describes statistically the error in concentration that occurs when the DDMT model is applied to predict transport through the embedded PFP network. The DDMT model is more accurate when the *RMSE* value decreases.

3. Results

[23] Using the models developed in section 2, we conducted a series of detailed numerical simulations that involve three different realizations of percolation-generated decimeter-wide PFP networks (Figure 1), a wide range of conductivity contrasts between high-K PFPs and low-K matrix, and varied diffusion coefficients. The first high-K network realization contains ~9% PFPs by volume, compared to ~20% and ~46% in the second and third realizations, respectively. Most simulations were conducted in the first realization and are referred to in this study as "base case", "Low K", "High K" and "ΔD^* @ K 100:1".

[24] In the "base case", the molecular diffusion coefficient in porous media is a typical value of some ions in pore fluid, 8.64×10^{-6} m^2/d. The PFP/matrix conductivity contrast was systematically adjusted from 10:1 to 200:1 while the effective conductivity of the dendritic PFP network-matrix system was maintained constant at 1.28 m/d. Table 1 provides the summary statistics of the K field at different conductivity contrasts.

[25] The Peclet number of the dendritic network system is calculated as

$$P_e = {K_N I L}\Big/{n D^*}. \tag{9}$$

In the base case the effective PFP network-matrix conductivity K_N is 1.28 m/d; the ambient gradient I is 0.001; the representative PFP width L is 0.1 m; and porosity n is 0.2. The Peclet number P_e is computed as 74, indicating a relative dominance of advective over diffusive processes in the dendritic PFP network system.

[26] In the "Low K" case, the magnitudes of both PFP and matrix conductivities were decreased to one ninth of their original values. As a result, the effective PFP-matrix conductivity K_N and Peclet number P_e are one ninth of the base-case values, which indicates a ninefold relative increase in the effect of diffusion. In the "High K" case, by contrast, conductivity values were increased 50 times, representing a decrease in the effect of diffusion to one-fiftieth of its original level. In both the "Low K" and "High K" cases the conductivity contrast was varied from 10:1 to 200:1. In the "ΔD^* @ K 100:1" case, the PFP/matrix conductivity contrast was fixed at 100:1 while the diffusion coefficient was varied from $1/3 \times D^*$ to $9 \times D^*$, where D^* is the base-case value of 8.64×10^{-6} m^2/d.

[27] In the source configuration investigated here, solute mass is proportioned on the basis of the hydraulic conductivity value of the PFPs versus the value for the matrix in the true detailed network model. For the corresponding DDMT model, initial solute mass is only distributed in the mobile zone given that in the immobile zone, no advective flow occurs and solute can only move in or out through the mass exchange with the mobile zone. The initial total mass is identical between the true network and DDMT models.

[28] Figure 2 compares the plume obtained from the PFP network system with that from the DDMT model at a conductivity contrast of 100:1 in the base case. Figure 2a shows the "true" concentration distribution in 3-D at time 0.13 pore volume that develops through the PFP network. Part of the plume is cut away for the ease of visualization. Solute spreading is asymmetric with most mass skewed to the upstream. The local shape of the plume is dominated by the geometric distribution of the PFP network. Figure 2b presents the equivalent 3-D plume simulated by the DDMT model. The calculated *RMSE* is 0.435 reflecting the quality of overall match between the network and the DDMT plumes. Direct visual comparison between the PFP network and DDMT plumes is also provided in Figure 2c, where the 2-D contours are vertically averaged from the 3-D concentrations. Despite the local point-to-point mismatch due to

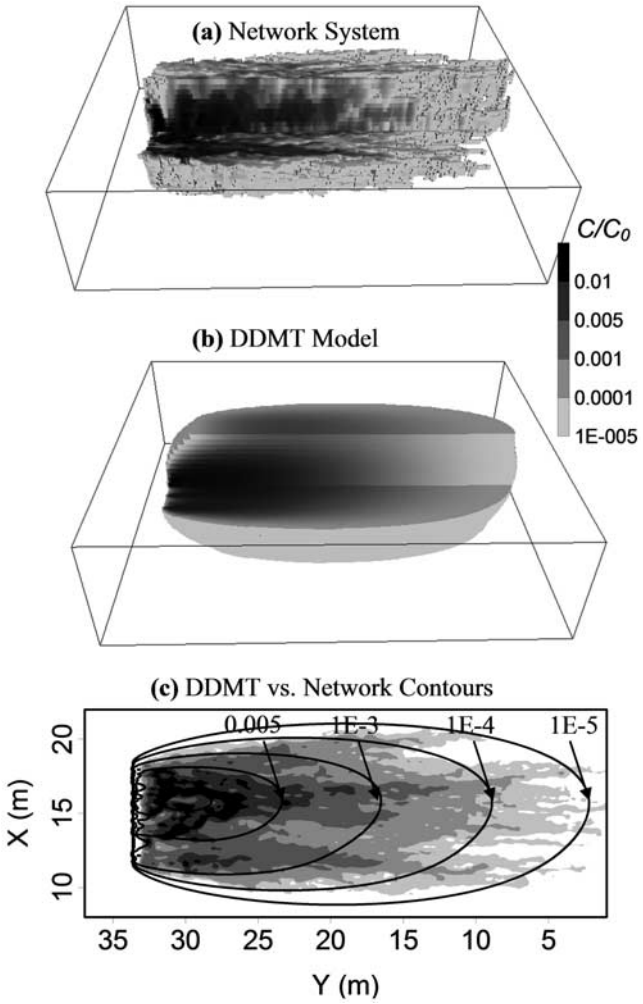

Figure 2. Comparison of plume matches by the DDMT model at a conductivity contrast of 100:1 in the base case: (a) 3-D network plume, (b) equivalent DDMT plume, and (c) 2-D network versus DDMT contours. Fill contours represent the true network model; line contours represent the DDMT model. The 2-D contours are vertically averaged from the original 3-D plume snapshots at time 0.13 pore volume.

the use of an effective conductivity field, the DDMT model provides a reasonable representation of the overall solute spreading pattern in the PFP network. Specifically, the DDMT model is able to reproduce both the near-source peak and low-concentration spreading in the downstream area.

[29] Figure 3 compares the plumes obtained from the true network model with those from the DDMT model at different PFP/matrix conductivity contrasts examined in the base case. Parameter values used to generate Figure 3 are listed in Table 2. The values of mobile porosity fraction and mass transfer rate coefficient were calculated using (4) and (5), respectively. Figure 3 demonstrates that the DDMT model provides a more reasonable representation of the average behavior of PFP network transport processes when the PFP/matrix conductivity contrast increases.

[30] Table 3 shows the computed *RMSE* values for the true network versus DDMT plumes at the different conductivity contrasts in the base case. Note that when the PFP/matrix conductivity contrast is small, the applicability of the DDMT model becomes poor, as displayed visually by the large mismatch in the near-source area (Figure 3). However, when contrasts between the high-K PFPs and the low-K matrix are larger, the accuracy of the DDMT model improves rapidly until the contrast reaches 150:1. When the PFP/matrix conductivity contrast increases beyond 150:1, no further significant improvement is observed. If one is willing to accept an *RMSE* $\sim$0.5 as a criterion, the DDMT model may be suitable for representing the PFPs under field conditions when the PFP/matrix conductivity contrast is determined to be $\sim$100:1 or greater.

[31] The effects of the PFP/matrix conductivity contrast on the applicability of the DDMT model are mostly evident in the near-source area. The larger the PFP/matrix conductivity contrast, the better the match of the DDMT model in the near-source area. As shown in Figure 3, for example, at a 10:1 conductivity contrast, there is no mass 3 m downgradient from the source in the PFP-network system, while in the DDMT model solute spreading is continuously present in the area. This near-source mismatch is reduced when the conductivity contrast increases. This is due to better meeting the key assumption of the DDMT model that the relatively slow-moving fluid in the low-K matrix can be regarded as completely immobile. When the conductivity contrast increases, the flow velocity in the low-K matrix becomes progressively smaller, and conceptually, the DDMT model becomes a better approximation.

[32] To further demonstrate the relation between the conductivity contrast and the near-source match by the DDMT model, we plotted the 1-D mass distribution profiles calculated by equation (7), wherein the 3-D solute plumes were integrated over each cross section i perpendicular to flow, relative to initial source mass. The calculated 1-D integrated mass profiles for the network and DDMT models in the base-case conductivity contrast suite are presented in Figure 4. It can be seen that when the PFP/matrix conductivity contrast increases, solute spreading is more dispersed and extends further into the downgradient area, and there is an increasing amount of local oscillation along the mass profile. Similar to the 2-D contours (Figure 3), as the conductivity contrast becomes larger, the DDMT model provides a better representation of the integrated mass distribution in the detailed network, particularly in the near-source region.

4. Discussion

4.1. PFP-Matrix Mass Transfer

[33] The mass transfer process between the low-K matrix and high-K PFPs consists of two different components, molecular diffusion and slow advective transport limited by the low-K matrix. The matrix-limiting slow advection is controlled by the conductivity contrast between the high-K PFPs and low-K matrix and the particular geometry of the dendritic PFP network. Diffusion, on the other hand, depends on the magnitude of the diffusion coefficient relative to the flow velocities in the PFP network system.

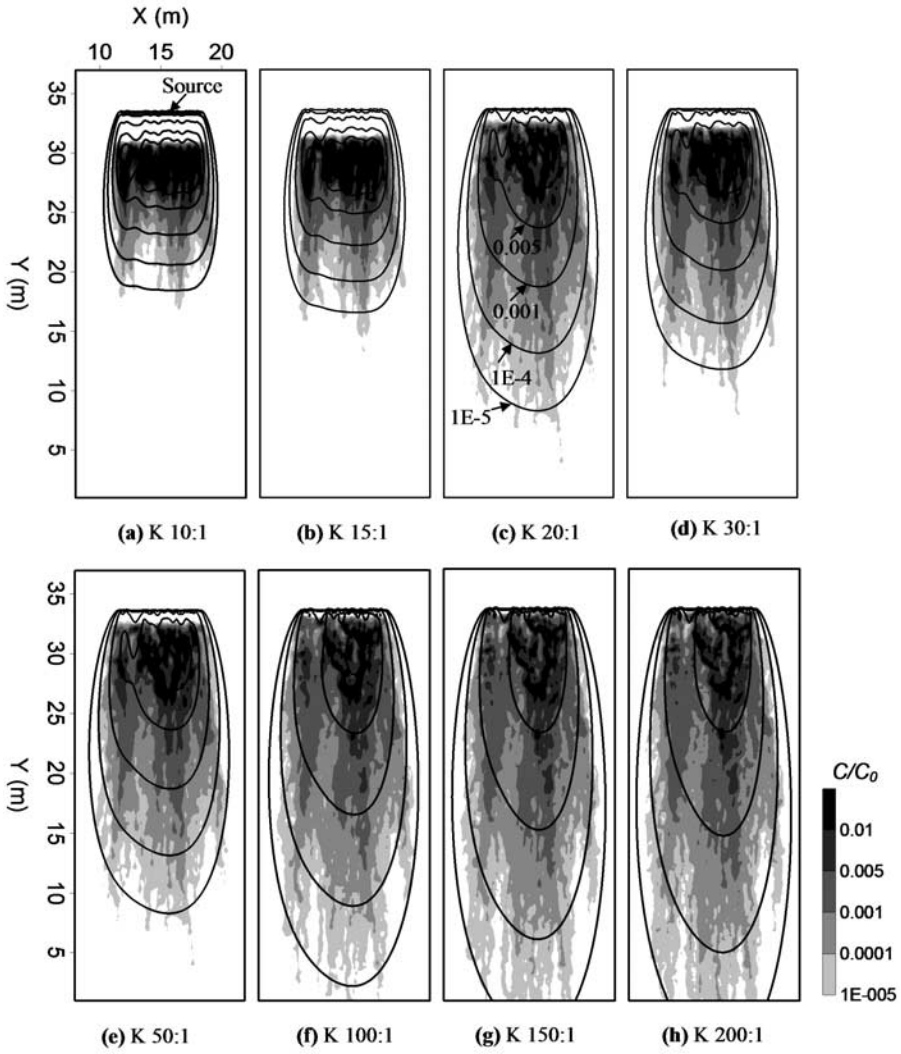

Figure 3. Plume matches by the DDMT model at different PFP/matrix conductivity contrasts in the base case. Simulation time is 0.13 pore volume. The calculated *RMSE* for each conductivity contrast is presented in Table 3.

4.1.1. Matrix-Limiting Slow Advection

[34] Effects of the matrix-limiting advection were explored from two perspectives: (1) changing the geometry of PFP network while maintaining the PFP/matrix conductivity contrast and diffusion rate constant and (2) changing the PFP/matrix conductivity contrast while maintaining the PFP geometry and molecular diffusion coefficient. With $D^* = 8.64 \times 10^{-6}$ m^2/d and the PFP/matrix conductivity

Table 2. Parameter Values Used to Produce the Plumes Shown in Figure 3[a]

PFP/Matrix K Constrast	True PFP Network Model				DDMT Model			
	K_N, m/d	K_C,[b] m/d	K_M,[b] m/d	K,[c] m/d	Φ[d]	n_m[d]	n_{im}[d]	ξ[e]
10:1	1.28	8.34	0.83	1.28	0.060	0.012	0.188	25.2
15:1	1.28	10.76	0.72	1.28	0.056	0.011	0.189	19.7
20:1	1.28	12.66	0.63	1.28	0.054	0.011	0.189	15.6
30:1	1.28	15.48	0.52	1.28	0.051	0.010	0.190	12.0
50:1	1.28	19.14	0.38	1.28	0.048	0.010	0.190	9.00
100:1	1.28	24.00	0.24	1.28	0.044	0.009	0.191	6.00
150:1	1.28	26.75	0.18	1.28	0.042	0.008	0.192	4.80
200:1	1.28	28.68	0.14	1.28	0.040	0.008	0.192	4.44

[a]Other important parameters not listed include molecular diffusion coefficient D^*, 8.64×10^{-6} m^2/d; total porosity n, 0.2; and ambient hydraulic gradient i, 0.001.
[b]Adjusted to maintain a constant K_N across different conductivity ratios.
[c]Conductivity field is uniform in the DDMT model and set equal to K_N.
[d]$n_m = \Phi \times n$; $n_{im} = (1 - \Phi) \times n$; Φ is calculated using (4).
[e]ξ is calculated using (5). The unit of ξ is in $\times 10^{-4}$ d^{-1}.

Table 3. Calculated *RMSE* for the Network Versus Equivalent DDMT Plumes at Different PFP/Matrix Conductivity Contrasts in the Base Case

PFP/Matrix K Contrast	RMSE for DDMT Versus Network
10:1	0.851
15:1	0.781
20:1	0.733
30:1	0.648
50:1	0.545
100:1	0.435
150:1	0.288
200:1	0.287

contrast at 50:1, the PFP volumetric fraction was increased from 9% to 46% in three network realizations (Figure 1). Figure 5 shows the transport behavior simulated from these different PFP geometries. As the PFP fraction increases, the solute plume becomes more symmetric. The extensive downgradient low-concentration tail evident in realization 1 no longer occurs in realization 3. This can be explained from two angles. First, when the PFP fraction increases, less mass is initially distributed in the low-K matrix. At the conductivity contrast of 50:1, the percentage of source mass in the matrix is 17% for realization 1, as compared to 7% in realization 2, and 2% in realization 3. Note that the mass initially distributed in the low-K matrix has to be transferred into nearby high-K PFPs before it can move more rapidly downstream. When the PFP fraction is large, as there is already significant mass initially distributed in the PFPs, the slow transfer of the limited source mass out of the low-K matrix is not as influential. Consequently, the plume is less asymmetric as it moves downgradient. Second and more importantly, when there are more PFPs, the matrix-limiting advective mass exchange is enhanced because the average distance a solute particle has to travel between the matrix and PFPs is reduced. As a result, the calculated mass transfer rate coefficient in the DDMT model increases from 9.0 $\times$

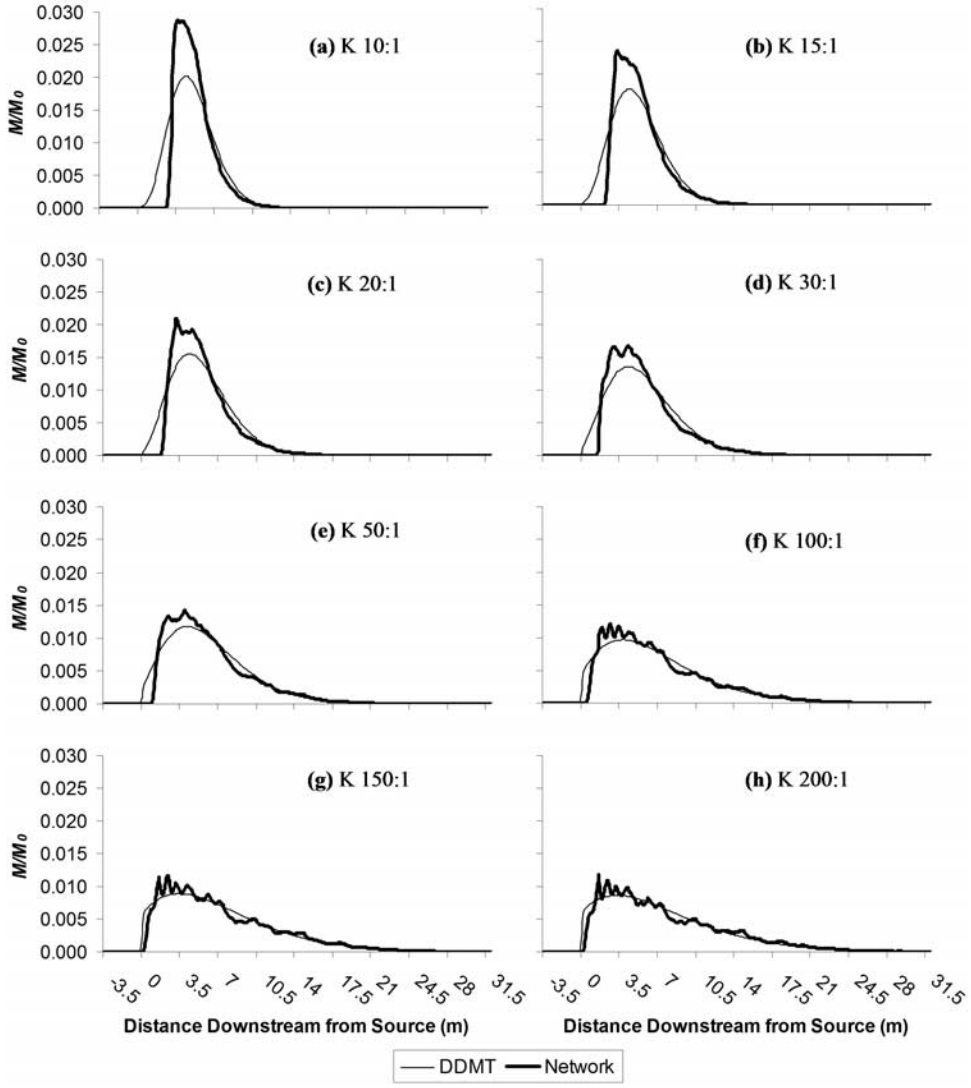

Figure 4. One-dimensional integrated mass distribution profiles of the PFP network and equivalent DDMT plumes at different PFP/matrix conductivity contrasts in the base case. Simulation time is 0.13 pore volume.

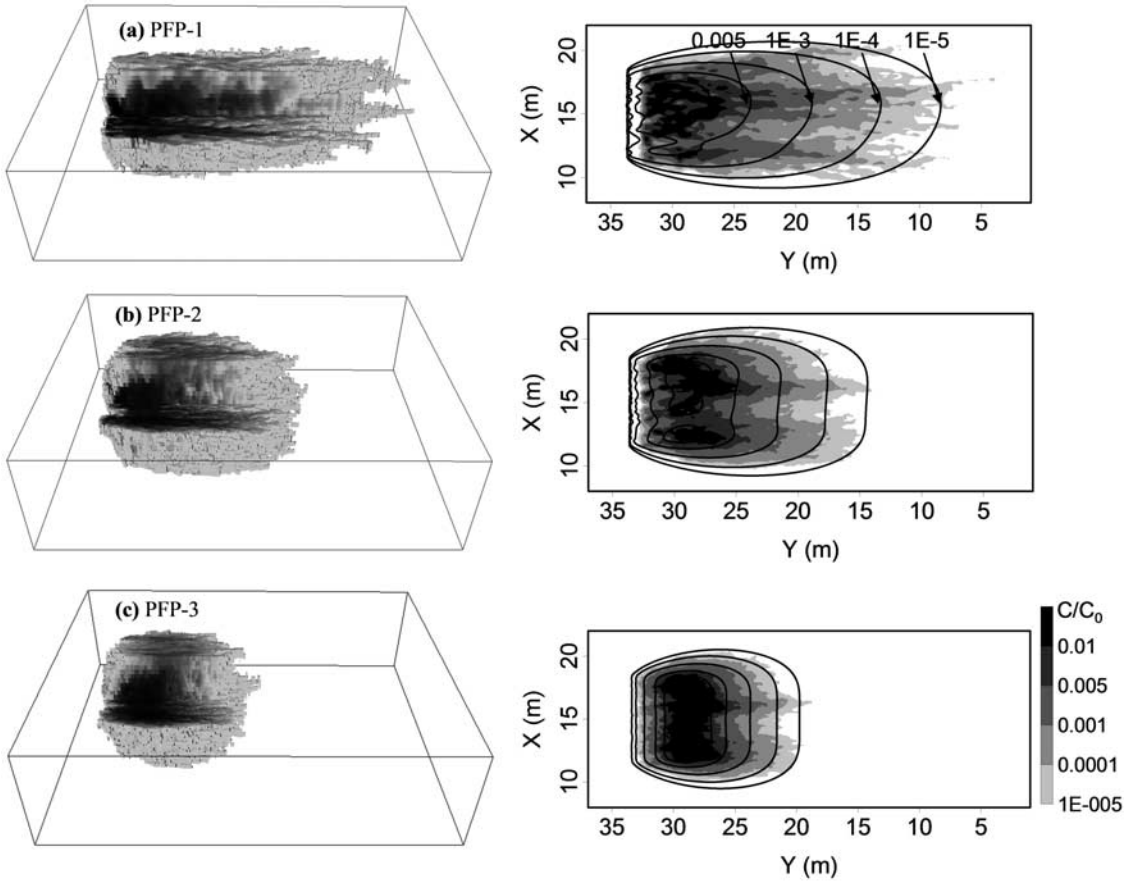

Figure 5. Plume comparison among different PFP network realizations at a constant PFP/matrix conductivity contrast of 50:1. Simulation time is 0.13 pore volume. The calculated mass transfer rate coefficient in the DDMT model is 9.0×10^{-4} d^{-1} in realization 1, 15.4×10^{-4} d^{-1} in realization 2, and 27.6×10^{-4} d^{-1} in realization 3.

10^{-4} d^{-1} in realization 1 to 27.6×10^{-4} d^{-1} in realization 3. In addition, the calculated *RMSE* between the network and DDMT plumes is 0.545 in realization 1, 0.433 in realization 2 and 0.197 in realization 3, indicating that the applicability of DDMT model improves with the increase in PFP fraction.

[35] Within each PFP network realization, PFP-matrix advective mass transfer is controlled by the conductivity contrast between the high-K PFPs and the low-K matrix. As shown in Figures 3 and 4, when the conductivity contrast increases, the true network plume is more asymmetric and skewed upstream. This is because the rate of PFP-matrix advective mass exchange becomes smaller when the relative magnitudes of the conductivities in the low-K matrix decline (see Table 1). The decreasing rate of matrix-limiting advective mass exchange with increasing conductivity contrasts is further substantiated by values in Table 2 where the calculated mass transfer rate coefficient decreases from 25.2×10^{-4} d^{-1} to 4.44×10^{-4} d^{-1} when the PFP/matrix conductivity contrast increases from 10:1 to 200:1.

4.1.2. Diffusion

[36] Because of the particular importance of diffusional mixing in media containing connected high-K networks [*LaBolle and Fogg*, 2001; *Zinn and Harvey*, 2003; *Liu et al.*, 2004], we explored the effects of diffusion using three sets of experiments, "Low K", "High K", and "ΔD^* @ K 100:1", as mentioned at the beginning of section 3. Figure 6 displays the comparison of plumes using different diffusion rate coefficients in the "ΔD^* @ K 100:1" case. The molecular diffusion coefficient was varied from $1/3 \times D^*$ to $9 \times D^*$, where D^* is the base-case diffusion coefficient, 8.64×10^{-6} m^2/d. When the diffusion coefficient increases, the plume becomes less asymmetric as preferential transport of solutes in the PFP network system is balanced by diffusive mass transfer between PFPs and the matrix. Furthermore, the roughness in the solute distribution that is evident using the diffusion coefficient of $1/3 \times D^*$ in the network model is significantly reduced at $9 \times D^*$. Corresponding to the increase in molecular diffusion coefficient value, the mass transfer rate coefficient in the DDMT model increases from 5.4×10^{-4} d^{-1} for $1/3 \times D^*$ to 8.4×10^{-4} d^{-1} for $9 \times D^*$. The calculated *RMSE* between the DDMT and network plumes declines as the diffusion coefficient value is increased, suggesting that the DDMT approximation becomes more appropriate for systems and solutes with higher molecular diffusion coefficients. Consistent results were obtained in the "Low K" and "High K" simulations.

4.2. DDMT Parameter Analysis

[37] The two DDMT parameters, the fraction of mobile porosity Φ and the mass transfer rate coefficient ξ, are typically treated as fitting parameters in common modeling applications [*Feehley et al.*, 2000; *Harvey and Gorelick*,

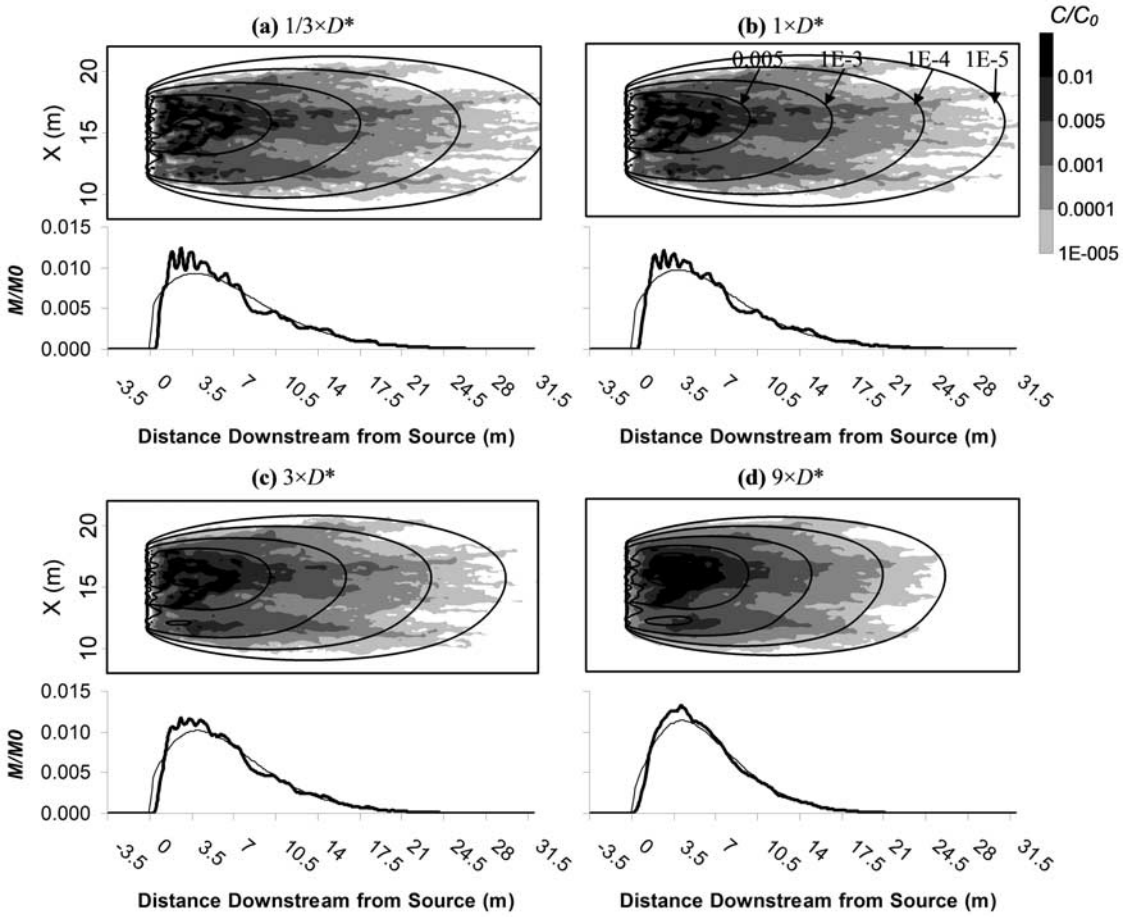

Figure 6. Plume comparison among different diffusion coefficients at a constant PFP/matrix conductivity contrast of 100:1 in PFP network realization 1. Simulation time is 0.13 pore volume. The base diffusion coefficient D^* is 8.64×10^{-6} m^2/d. The calculated *RMSE* for each diffusion coefficient is, in turn, (a) 0.414, (b) 0.435, (c) 0.333, and (d) 0.256. The mass transfer rate coefficient in the DDMT model is (a) 5.4×10^{-4} d^{-1}, (b) 6.0×10^{-4} d^{-1}, (c) 6.6×10^{-4} d^{-1}, and (d) 8.4×10^{-4} d^{-1}.

2000; *Haggerty et al.*, 2001]. For the synthetic aquifers investigated in this work (based on three PFP realizations), we demonstrate that these parameters can be directly determined on a physical basis using equations (4) and (5), respectively. Table 2 lists the calculated values of DDMT parameters for the base-case conductivity contrast suite.

[38] Calculation of Φ only involves different representative conductivity values in the PFP network system (see equation (4)). Two observations can be made regarding Φ. First, the calculated value of Φ is always smaller than the actual volumetric percentage, 9%, of high-K PFPs in the network system. This is because the distribution of PFPs in the network is dendritic and contains some dead-end branches that do not function as the main conduits to transport solute. When the dendritic network (with effective conductivity K_N) is translated into straight PFP conduits (with conductivity K_C) embedded in the low-K matrix (with conductivity K_M), a significant portion of PFPs are effectively removed. Recall that in this work we used the volumetric percentage, R, of straight PFP conduits to approximate the fraction of mobile porosity in the DDMT model. Second, for a given PFP network, Φ declines with the increase in conductivity contrast and appears to converge to an asymptotic value when the conductivity contrast is sufficiently high. This is because when the conductivity contrast increases, the flow velocities in the straight PFP conduits (i.e., $K_C IA$ in equation (3)) increase while the flow velocities in the low-K matrix (i.e., $K_M IA$ in equation (3)) decrease. As shown in Table 2, the increase in K_C is larger than the decrease in K_M, and R becomes small as the total flow rate (i.e., $K_N IA$ in equation (3)) has to remain identical to maintain equivalency among different conductivity contrasts. From Table 2 it is noteworthy that the increase in K_C becomes progressively less significant as the PFP/matrix conductivity contrast becomes large. For example, the relative increase in K_C is 1.93 m/d when the conductivity contrast increases from 150:1 to 200:1, compared to 2.75 m/d when the contrast increases from 100:1 to 150:1. Therefore, when the conductivity contrast is sufficiently high, such as in a fractured rock system, the conductivity in the matrix is so small that it can be treated practically as zero, the increase in K_C shall become negligible, leading to an asymptotic value for the estimated Φ for a given PFP network.

[39] Table 2 shows that ξ decreases with increasing conductivity contrasts between high-K PFPs and low-K matrix. This is because, as discussed in section 4.1.1, the rate of matrix-limiting advective mass exchange decreases

with increasing PFP/matrix conductivity contrasts. When the diffusion rate coefficient increases from $1/3 \times D^*$ (i.e., 2.88×10^{-6} m^2/d) to $9 \times D^*$ (7.78×10^{-5} m^2/d) at a PFP/matrix conductivity contrast of 100:1 in the base case, ξ increases from 5.4×10^{-4} d^{-1} to 8.4×10^{-4} d^{-1} (Figure 6). Across different PFP network realizations, ξ generally increases with the volumetric fraction of PFPs (Figure 5).

5. Summary and Conclusions

[40] This study explores the efficacy of the DDMT model to characterize transport in the presence of decimeter-scale PFPs to a 3-D binary heterogeneous flow system involving an embedded dendritic network. Numerical experiments covered a range of flow and transport conditions including a suite of PFP/matrix conductivity contrasts varying from 10:1 to 200:1, different geometries of the PFP network, different magnitudes of effective conductivities and diffusion rate coefficients.

[41] The DDMT model reproduced both the near-source peak and low-concentration tail in the downstream area resulting from transport through the PFPs when the conductivity contrasts between high-K PFPs and low-K matrix were relatively significant. When the conductivity contrast increases, the flow velocity in the low-K matrix becomes progressively smaller, and the discrepancy associated with the DDMT model becomes less significant. This is because the inherent limitation of the DDMT model, which treats relatively slow-moving fluid in the low-K matrix as completely immobile, is minimized.

[42] The DDMT model was shown to match the true network system better when molecular diffusion coefficients were higher. When the diffusion coefficient values were increased, the plume became less asymmetric as preferential transport of solutes in the PFP network system was balanced by diffusive mass transfer between PFPs and the matrix, and the solute profile showed less roughness. As the volumetric fraction of PFPs was increased, the plume was generally less asymmetric. This is because (1) there is already significant mass initially distributed in the PFPs and the slow transfer of the limited source mass out of the low-K matrix is not as influential, and (2) the matrix-limiting advective mass exchange is enhanced as the average distance a solute particle must travel between the matrix and PFPs is reduced. The DDMT model became more effective in representing the network system when there were more PFPs.

[43] Our results have provided some insights into the DDMT model parameters. While they are typically treated as fitting parameters, in this work the fraction of mobile porosity Φ and mass transfer rate coefficient ξ are directly computed on the basis of physical relations (4) and (5) without resorting to model calibration. Φ is generally smaller than the actual volumetric proportion of PFPs owing to the tortuous nature of PFPs. As the PFP/matrix conductivity contrast increases, the Φ value declines and appears to converge to an asymptotic value when the conductivity contrast is sufficiently high. ξ is controlled by two different processes, i.e., the matrix-limiting slow advection and molecular diffusion. The greater the diffusion coefficient value, the larger the ξ value in the DDMT model. When the PFP/matrix conductivity contrast increases or the volumetric fraction of PFPs decreases, the ξ value becomes smaller because the rate of matrix-limiting advective mass exchange decreases.

[44] **Acknowledgments.** This material is based upon work supported by the National Science Foundation under grants EAR-0538011 and EAR-0537668. Any opinions, findings, and conclusions or recommendations expressed in this material are those of the author(s) and do not necessarily reflect the views of the National Science Foundation. Additional support was provided by a GSA student research grant, the University of Alabama Graduate Council Fellowship, and the Department of Geological Sciences Research Funds.

References

Barlebo, H. C., M. C. Hill, and D. Rosbjerg (2004), Investigating the Macrodispersion Experiment (MADE) site in Columbus, Mississippi, using a three-dimensional inverse flow and transport model, *Water Resour. Res.*, *40*, W04211, doi:10.1029/2002WR001935.

Benson, D. A., S. W. Wheatcraft, and M. M. Meerschaert (2000), The fractional-order governing equation of Levy motion, *Water Resour. Res.*, *36*(6), 1413–1423.

Berkowitz, B., and H. Scher (1998), Theory of anomalous chemical transport in fracture networks, *Phys. Rev. E*, *57*(5), 5858–5869.

Berkowitz, B., J. Klafter, R. Metzler, and H. Scher (2002), Physical pictures of transport in heterogeneous media: Advection-dispersion, random-walk, and fractional derivative formulations, *Water Resour. Res.*, *38*(10), 1191, doi:10.1029/2001WR001030.

Berkowitz, B., A. Cortis, M. Dentz, and H. Scher (2006), Modeling non-Fickian transport in geological formations as a continuous time random walk, *Rev. Geophys.*, *44*, RG2003, doi:10.1029/2005RG000178.

Boggs, J. M., and E. E. Adams (1992), Field study of dispersion in a heterogeneous aquifer: 4. Investigation of adsorption and sampling bias, *Water Resour. Res.*, *28*(12), 3325–3336.

Boggs, J. M., S. C. Young, L. M. Beard, L. W. Gelhar, K. R. Rehfeldt, and E. E. Adams (1992), Field study of dispersion in a heterogeneous aquifer: 1. Overview and site description, *Water Resour. Res.*, *28*(12), 3281–3291.

Boggs, J. M., L. M. Beard, S. E. Long, M. P. McGee, W. G. MacIntyre, C. P. Antworth, and T. B. Stauffer (1993), Database for the Second Macrodispersion Experiment (MADE-2), *Tech. Rep. TR-102072*, Electr. Power Res. Inst., Palo Alto, Calif.

Falta, R. W. (2000), Numerical modeling of kinetic interphase mass transfer during air sparging using a dual-media approach, *Water Resour. Res.*, *36*(12), 3391–3400.

Feehley, C. E., C. Zheng, and F. J. Molz (2000), A dual-domain mass transfer approach for modeling solute transport in heterogeneous porous media, application to the MADE site, *Water Resour. Res.*, *36*(9), 2051–2515.

Gorelick, S. M., G. Liu, and C. Zheng (2005), Quantifying mass transfer in permeable media containing conductive dendritic networks, *Geophys. Res. Lett.*, *32*, L18402, doi:10.1029/2005GL023512.

Gwo, J. P., P. M. Jardine, G. V. Wilson, and G. T. Yeh (1995), A multiple-pore-region concept to modeling mass transfer in subsurface media, *J. Hydrol*, *164*, 217–237.

Haggerty, R., and S. M. Gorelick (1995), Multiple-rate mass transfer for modeling diffusion and surface reactions in media with pore-scale heterogeneity, *Water Resour. Res.*, *31*(10), 2383–2400.

Haggerty, R., S. W. Fleming, L. C. Meigs, and S. A. McKenna (2001), Tracer tests in a fractured dolomite: 2. Analysis of mass transfer in single-well injection-withdrawal tests, *Water Resour. Res.*, *37*(5), 1129–1142.

Harbaugh, A. W., E. R. Banta, M. C. Hill, and M. G. McDonald (2000), *MODFLOW-2000, the U.S. Geological Survey Modular Ground-Water Model—User Guide to Modularization Concepts and the Ground-Water Flow Processes*, *U.S. Geol. Surv. Open File Rep.*, *00-92*, 121 pp.

Harvey, C. F., and S. M. Gorelick (2000), Rate-limited mass transfer or macrodispersion: Which dominates plume evolution at the Macrodispersion Experiment (MADE) site?, *Water Resour. Res.*, *36*(3), 637–650.

Hill, M. C., H. C. Barlebo, and D. Rosbjerg (2006), Reply to comment by F. Molz et al. on "Investigating the Macrodispersion Experiment (MADE) site in Columbus, Mississippi, using a three-dimensional inverse flow and transport model," *Water Resour. Res.*, *42*, W06604, doi:10.1029/2005WR004624.

Kirchner, J. W., X. Feng, and C. Neal (2000), Fractal stream chemistry and its implications for contaminant transport in catchments, *Nature*, *403*, 524–527.

LaBolle, E. M., and G. E. Fogg (2001), Role of molecular diffusion in contaminant migration and recovery in an alluvial aquifer system, *Transp. Porous Media*, *42*, 155–179.

Liu, G., C. Zheng, and S. M. Gorelick (2004), Limits of applicability of the advection-dispersion model in aquifers containing connected high-

conductivity channels, *Water Resour. Res.*, *40*, W08308, doi:10.1029/2003WR002735.

McKenna, S. A., L. C. Meigs, and R. Haggerty (2001), Tracer tests in a fractured dolomite: 3. Double-porosity, multiple-rate mass transfer processes in convergent flow tracer tests, *Water Resour. Res.*, *37*(5), 1143–1154.

Molz, F. J., C. Zheng, S. M. Gorelick, and C. F. Harvey (2006), Comment on "Investigating the Macrodispersion Experiment (MADE) site in Columbus, Mississippi, using a three-dimensional inverse flow and transport model" by Heidi Christiansen Barlebo, Mary C. Hill, and Dan Rosbjerg, *Water Resour. Res.*, *42*, W06603, doi:10.1029/2005WR004265.

Ronayne, M. J., and S. M. Gorelick (2006), Effective permeability of porous media containing branching channel networks, *Phys. Rev. E*, *73*, 026305, 1–10.

Scher, H., G. Margolin, R. Metzler, J. Klafter, and B. Berkowitz (2002), The dynamical foundation of fractal stream chemistry: The origin of extremely long retention times, *Geophys. Res. Lett.*, *29*(5), 1061, doi:10.1029/2001GL014123.

Stark, C. P. (1991), An invasion percolation model of drainage network evolution, *Nature*, *352*, 423–425.

Wang, P. P., C. Zheng, and S. M. Gorelick (2005), A general approach to advective-dispersive transport with multirate mass transfer, *Adv. Water Resour.*, *28*, 33–42.

Zheng, C. (2006), *MT3DMS v5.2 Supplemental User's Guide*, Dept. of Geol. Sci., Univ. of Ala., Tuscaloosa.

Zheng, C., and G. D. Bennett (2002), *Applied Contaminant Transport Modeling*, 2nd ed., 621 pp., John Wiley, New York.

Zheng, C., and J. J. Jiao (1998), Numerical simulation of tracer tests in a heterogeneous aquifer, *J. Environ. Eng.*, *124*(6), 510–516.

Zheng, C., and P. P. Wang (1999), *MT3DMS: Documentation and User's Guide, Contract Rep. SERDP-99–1*, U.S. Army Eng. Res. and Dev. Cent., Vicksburg, Miss.

Zinn, B., and C. F. Harvey (2003), When good statistical models of aquifer heterogeneity go bad: A comparison of flow, dispersion, and mass transfer in connected and multivariate Gaussian hydraulic conductivity fields, *Water Resour. Res.*, *39*(3), 1051, doi:10.1029/2001WR001146.

S. Gorelick, Department of Environmental Earth System Science, Stanford University, Stanford, CA 94305, USA. (gorelick@stanford. edu)

G. Liu, Kansas Geological Survey, University of Kansas, 1930 Constant Avenue, Lawrence, KS 66047-3726, USA. (gliu@kgs.ku.edu)

C. Zheng, Department of Geological Sciences, University of Alabama, 202 Bevill Building, Box 870338, Tuscaloosa, AL 35487-0338, USA. (czheng@ua.edu)